Journal of Applied Physics

RESEARCH ARTICLE | OCTOBER 15 2014

Optical simulation and optimization of weak-microcavity tandem white organic light-emitting diodes

Shouzhen Yue; Runda Guo; YuKun Wu; Pingrui Yan; Shiming Zhang; Zhensong Zhang; Dalong Qu; Yi Zhao

J. Appl. Phys. 116, 153102 (2014)
https://doi.org/10.1063/1.4897365

Optical simulation and optimization of weak-microcavity tandem white organic light-emitting diodes

Shouzhen Yue,[1] Runda Guo,[1] YuKun Wu,[1] Pingrui Yan,[1] Shiming Zhang,[2] Zhensong Zhang,[1] Dalong Qu,[1] and Yi Zhao[1,a)]
[1]*State Key Laboratory on Integrated Optoelectronics, College of Electronic Science and Engineering, Jilin University, Changchun 130012, People's Republic of China*
[2]*Département of Chemical Engineering, École Polytechnique de Montréal, Montréal, Québec H3C 3J7, Canada*

(Received 24 June 2014; accepted 22 September 2014; published online 15 October 2014)

We systematically studied the influence of weak microcavity effects on the optical properties of tandem white organic light-emitting diodes (WOLEDs) using optical simulation. Based on the simulation results, an image processing method is developed and verified for rational design of high-performance tandem WOLEDs. The results indicate that low operating voltage, good color rendering index, and angular emission properties can be simultaneously obtained in tandem WOLEDs by engineering the device structure. This study provides promising direction for the development of high-performance tandem WOLEDs. © *2014 AIP Publishing LLC*.
[http://dx.doi.org/10.1063/1.4897365]

I. INTRODUCTION

Since white organic light-emitting diodes (WOLEDs) were first developed by Kido *et al.* in 1995,[1] they have attracted extensive interest because of their low power consumption, light weight, and flexibility. WOLEDs are being considered as a low-cost alternative for several applications such as large-area light sources, maskless fabrication of large-area full-color displays by coupling with color filters, and backlights for liquid-crystal displays. To date, tremendous progress has been realized in both science and technology to improve the performance of WOLEDs. In particular, tandem WOLEDs show great advantages in solid-state lighting because they can achieve high brightness at low current density with high efficiency and long lifetime.[2–5] Recently, tandem WOLEDs have also shown great potential as large flat-panel displays.[6–9]

Although many high-performance tandem WOLEDs have been reported,[3,10–14] to date, the optical properties of tandem WOLEDs, especially weak-microcavity devices, have not been well elaborated. In addition, the relationship between optical cavity effects and device characteristics is still not clear, which has restricted the development of high-performance tandem WOLEDs. To solve these problems, in this work, we performed a systematic simulation to study the optical properties of weak microcavities in tandem WOLEDs. The effect of device structure on optical characteristics is successfully clarified by varying the location of the recombination zone in the devices. The properties of tandem WOLEDs with exchanged emission zones are also examined. Based on our simulation results, a universal strategy for the determination of optimal device structure to realize high-performance tandem WOLEDs is proposed.

a)Author to whom correspondence should be addressed. Electronic mail: yizhao@jlu.edu.cn. Tel.: +86 431 85168242 8301.

II. EXPERIMENTAL

A. Device fabrication

We described the fabrication and measurement procedures in detail elsewhere.[15] All samples were fabricated without breaking vacuum and measured directly after fabrication in a glove box filled with ultra-high purity nitrogen containing <1 ppm water and oxygen. All materials were purchased from Luminescence Technology Corp. 4,4′,4″-Tris(3-methylphenylphenylamino)triphenylamine (m-MTDATA) and di-[4–(N,N-ditolyl-amino)-phenyl]cyclohexane (TAPC) were used as hole injection materials. The electron blocking material was tris(phenylpyrazole)iridium ($Ir(ppz)_3$); 4,7-diphenyl-1,10-phenanthroline (Bphen) was used as an electron transportation layer. The charge generation layer (CGL) was composed of Bphen:Cs_2CO_3 (3:1)/TAPC:MoO_x (3:1). Bis(3,5-difluoro-2–(2-pyridyl)phenyl-(2-carboxypyridyl)iridium (III) (FIrpic), and iridium (III) bis(4-phenylthieno[3,2-c]pyridinato-N,C2′)acetylacetonate (PO-01) were used as blue and yellow, respectively. The host materials for yellow and blue electrophosphorescent devices were 4,4′-N,N′-dicarbazole-biphenyl (CBP) and 1,3-bis(9-carbazolyl)benzene (mCP), respectively.

B. Simulation parameters

The simulated structures of weak-microcavity tandem WOLEDs (termed BY and YB) used in this study and reference B and Y devices are shown in Fig. 1.

In the BY (YB) device, the blue (yellow) emissive unit is located close to the ITO anode. To simplify our calculation, the average refractive index of all of the organic layers was assumed to be 1.7 including that of the organic p-n junction CGL.[16] The parameters used in the calculations are listed in Table I.

To model the tandem WOLEDs, the following simplifications were used. (i) Because the yellow unit (long

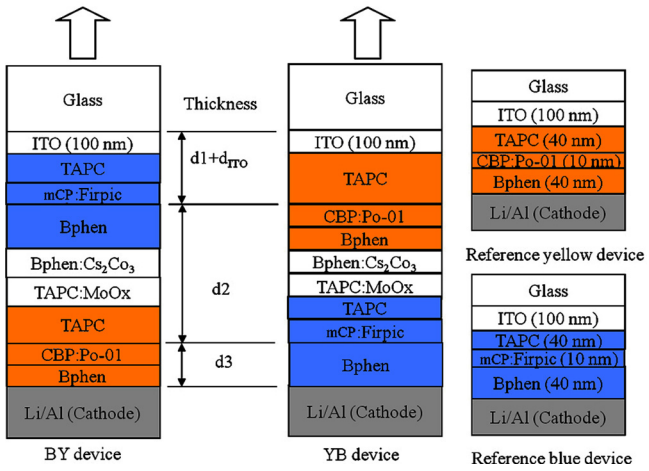

FIG. 1. The structures of tandem WOLEDs and reference monochrome devices used in our simulations.

wavelength) did not absorb much light from the blue unit (short wavelength) in our tandem WOLEDs (see experimental details in the supplementary material[18]), the emission intensities of each monochrome emitter were calculated separately, and then superimposed to yield the total emission spectra of the tandem WOLEDs. (ii) The calculations

TABLE I. Parameters used in the simulations.

Material	Aluminum	Organic material	ITO	Glass
Refractive index	N(λ)[a]	1.7[b]	1.8[b]	1.5[b]
Thickness	100 nm	(d1, d2, d3)[c]	100 nm	1 mm

[a]Variable. The Lorentz-Drude model is used to obtain the permittivity of aluminum at various wavelengths.
[b]Constant. Taken from the literature.[17]
[c]Variable. The ranges of d1, d2, and d3 are 0–200, 40–140, and 0–210, respectively.

ignored the far-field interference in the glass by assuming that the electric field exiting the glass/ITO interface was the same as that incident at the glass/air interface because the glass substrate is far thicker than the other layers (~1 mm).[19] (iii) In the simulations, the distribution areas of blue and yellow emitters were mainly located near the interfaces of mCP/Bphen and CBP/TCTA, respectively.

Light propagating in the resonant cavity will undergo both multiple-beam and wide-angle interference. Because weak microcavity effects dominate the performance of conventional tandem WOLEDs, the approximate theoretical emission spectrum of a single-stack device can be calculated using the following formula:[20]

$$|E_{out}^{(s,p)}(\lambda,\theta)|^2 = |E_{nc}(\lambda)|^2 \left(\frac{1 + r_1^{(s,p)} e^{-i\left(\frac{4\pi d\cos\theta}{\lambda} - \phi_{cathode}^{(s,p)}\right)}}{1 - r_1^{(s,p)} r_2^{(s,p)} e^{-i\left(4\pi l\cos\theta - \phi_{anode}^{(s,p)} - \phi_{cathode}^{(s,p)}\right)}} \right)^2 T_{glass}^{(s,p)} T_{air}^{(s,p)}. \quad (1)$$

Here, the superscript (s,p) represents the s-(p-) polarization. $|E_{nc}(\lambda)|^2$ is the normalized free space electroluminescent (EL) intensity; r_1, r_2 are the effective reflectivity of the cathode and anode sides, respectively, which were determined using the transfer matrix method; d, l are the optical lengths; $\phi_{anode}, \phi_{cathode}$ are the reflection phase shifts at the ITO and metal cathode sides, respectively. T_{glass}, T_{air} are the effective transmissivity at ITO/glass and glass/air interfaces, respectively. As depicted in Fig. 2, using the transfer matrix method, the reflectivity, transmissivity, and reflection phase shifts at each mirror can be calculated. Equation (1) allowed the external emission spectra to be calculated.

Then, the emission spectrum of a tandem WOLED can be expressed as

$$|E_{white}^{(s,p)}(\lambda,\theta)|^2 = \gamma_1 |E_{blue}^{(s,p)}(\lambda,\theta)|^2 + \gamma_2 |E_{yellow}^{(s,p)}(\lambda,\theta)|^2. \quad (2)$$

The device performance depends on both optical outcoupling and electrical properties, namely, a charge balance factor. In general, the electrical properties of blue and yellow devices are different. Thus, a better way to describe the emission spectrum of a tandem WOLED is to introduce a modified coefficient. As shown in Fig. 3, the values of γ_1 and γ_2 in Eq. (2) were obtained by comparing the spectra simulated using Eq. (1) with real experimental spectra of

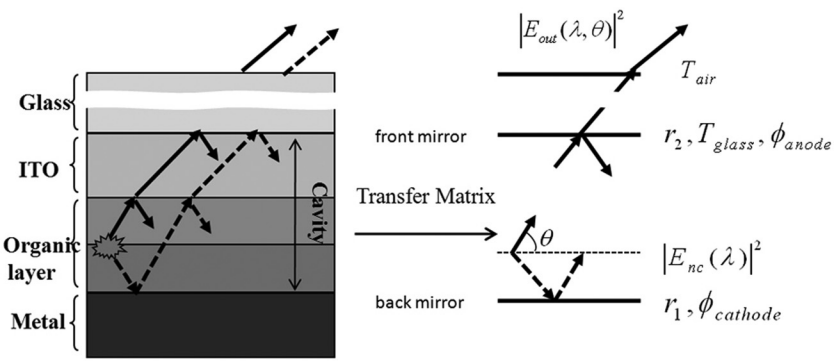

FIG. 2. Schematic figure of the optical physic process in the weak microcavity OLED.

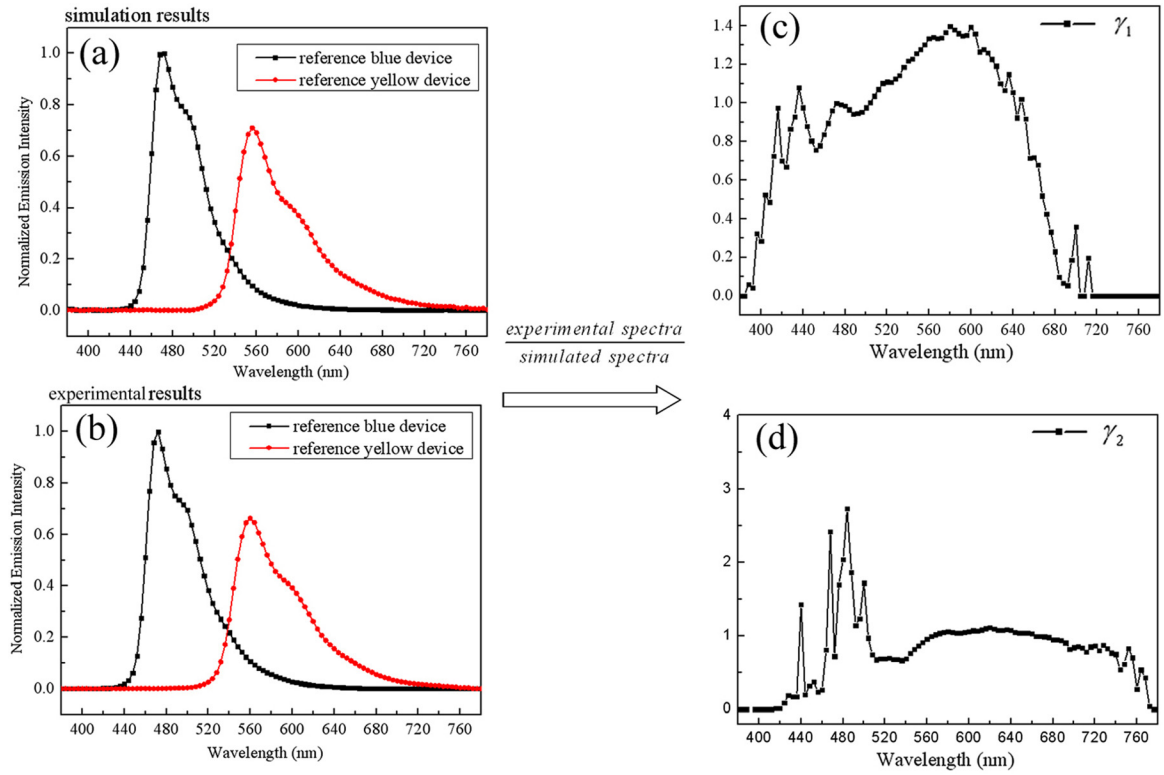

FIG. 3. The calculation process of γ_1 and γ_2.

individual blue and yellow devices at the same current density. That is, the effect of electrical properties on device performance was considered in this simulation and was represented by γ_1 and γ_2.

III. RESULTS AND DISCUSSION

A. Necessity of optical simulation for tandem WOLEDs

To illustrate the importance of optical simulation of tandem WOLEDs, we first fabricated device A1 by simply connecting blue and yellow OLEDs following traditional fabrication processes. Devices with the following structures were simulated. Device A1: ITO/m-MTDATA (30 nm)/$Ir(ppz)_3$ (10 nm)/mCP:FIrpic(10 wt. %, 15 nm)/Bphen (30 nm)/Bphen:Cs_2CO_3 (10 nm)/m-MTDATA:MoO_x (5 nm)/m-MTDATA (25 nm)/$Ir(ppz)_3$ (10 nm)/CBP:PO-01 (8 wt. %, 10 nm)/Bphen (40 nm)/LiF (1 nm)/Al; Device A2: ITO/m-MTDATA:MoO_x (5 nm)/m-MTDATA (25 nm)/$Ir(ppz)_3$ (10 nm)/CBP:PO-01 (8 wt. %, 10 nm)/Bphen (40 nm)/LiF (1 nm)/Al; Device A3: ITO/Bphen (30 nm)/Bphen:Cs_2Co_3 (10 nm)/m-MTDATA:MoO_x (5 nm)/m-MTDATA (25 nm)/$Ir(ppz)_3$ (10 nm)/CBP:PO-01 (8 wt. %, 10 nm)/Bphen (40 nm)/LiF (1 nm)/Al; Device A4: ITO/m-MTDATA (30 nm)/$Ir(ppz)_3$ (10 nm)/mCP:FIrpic (10 wt. %, 15 nm)/Bphen (30 nm)/Bphen:Cs_2Co_3 (10 nm)/LiF (1 nm)/Al.

Fig. 4 clearly shows that the FIrpic emission in tandem device A1 is strongly suppressed. This suppression may be attributed to the following three possibilities: (i) unfavorable CGL; (ii) poor performance of blue-emitting units; (iii) suppression of FIrpic emission by the microcavity effect. To study the underlying reason for the suppressed emission from FIrpic, devices A2, A3, and A4 were successively fabricated. The difference between devices A2 and A3 is that the CGL used in device A1 was employed as the HTL in device A3. Fig. 4 reveals that the emission spectra and efficiency of devices A2 and A3 are quite similar, which demonstrates the efficient operation of the CGL and thus possibility (i) can be excluded. The good performance of device A4 also proves the effective operation of the blue-emitting unit in device A1, which further excludes possibility (ii). Therefore, the suppressed blue emission in device A1 is

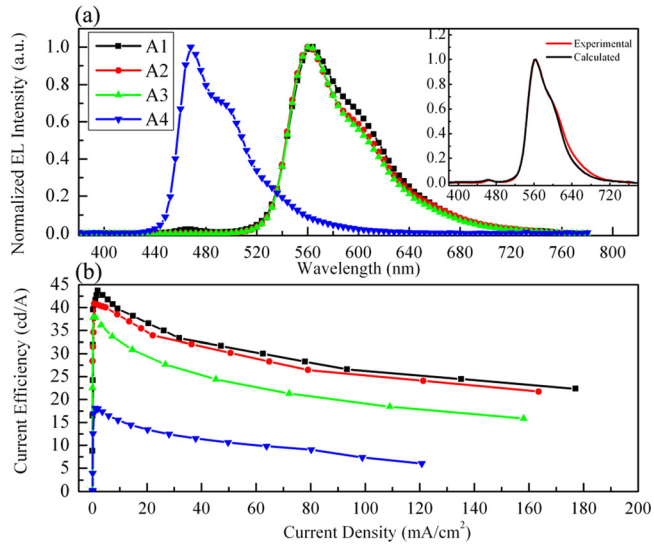

FIG. 4. (a) The normalized EL spectra of device A1-A4. The inset is comparison between experimental and calculated spectra. (b) The current efficiency properties of four devices.

determined to arise from the strong optical interference in the tandem device caused by the microcavity effect, i.e., possibility (iii). The above discussion indicates that, in addition to optimizing device structure, rational design of the optical microcavity is also required to obtain a tandem WOLED. The best way to predict a suitable optical microcavity in such devices is optical simulation.

B. Simulation of emission properties of tandem WOLEDs

The design of device structure for white-light applications is challenging because the emission spectrum needs to cover a wide range of the visible light region. Therefore, a trade-off among different emission colors is necessary to obtain both high efficiency and good color rendering index (CRI). Moreover, we observed that a comparable change in layer thickness caused quite different performance variation of the tandem WOLEDs when we exchanged the location of the emission zone. This observation is consistent with the work of Forrest *et al.*,[21] who found that the order of emissive units influences the color balance of tandem WOLEDs. With the goal of simulating white-light tandems WOLEDs, we first studied the optical properties of weak-microcavity tandem WOLEDs with exchanged emission zones.

1. Luminance intensity

Device efficiency is an essential parameter to evaluate OLED performance. The study of external luminance intensity will provide guidelines to obtain high-efficiency devices because the EL quantum yield is proportional to the intensity of external luminance. According to Eq. (2), the external luminance intensity of a tandem WOLED in the perpendicular direction can be expressed as

$$I_{out}^{white} = \frac{\int_{380}^{780} E_{white}^2 V(\lambda) d\lambda}{I_{ref}^{white}}$$

$$I_{ref}^{white} = \int_{380}^{780} \left(E_{ref\_blue}^2 + E_{ref\_yellow}^2 \right) V(\lambda) d\lambda, \quad (3)$$

where $V(\lambda)$ is a luminosity function and represents the way humans perceive brightness. The forward luminance ($\int_{380}^{780} E_{white}^2 V(\lambda) d\lambda$) is normalized to the reference value I_{ref}^{white}. Here, $E_{ref\_blue}^2$ and $E_{ref\_yellow}^2$ are experimental spectra of reference blue and yellow devices shown in Fig. 3(b), respectively. The typical method to optimize the total flux of light emission from monochrome devices is to match the total thickness to the resonance condition for the peak emission wavelength of the emitter.[22] However, this will suppress the emission of the other colors and thereby narrow the emission spectrum of a device. To reveal the underlying mechanism of flux variation, we first varied the total thickness of organic layers to optimize the total flux of light emission. Fig. 5 shows the color-filled contour diagrams of simulated external emission intensity (I_{out}^{white}) of two kinds of tandem devices with d2 increasing from 40 to 140 nm.

The simulated results in Fig. 5 show that the emission intensity is quite sensitive to the distance between two emissive units (d2). These results are reasonable because in tandem WOLEDs, the emission intensity strongly depends on layer thickness because of microcavity effects, as discussed above. High external luminance intensities ($I_{out}^{white} > 1.2$, white parts) are obtained at smaller d2 (~40 nm) or larger d2 (~120 nm). However, when d2 is around 80 nm, the total emission intensity is weaker than the reference value (i.e., I_{ref}^{white}) for both BY and YB devices. Within the variation region of d1, d2, and d3, I_{out}^{white} in the BY device can reach 1.4 when (d1, d2, d3) = (110, 140, 75), and 1.25 for (70, 40, 50). For the YB device, I_{out}^{white} can reach 1.37 at both (75, 40,

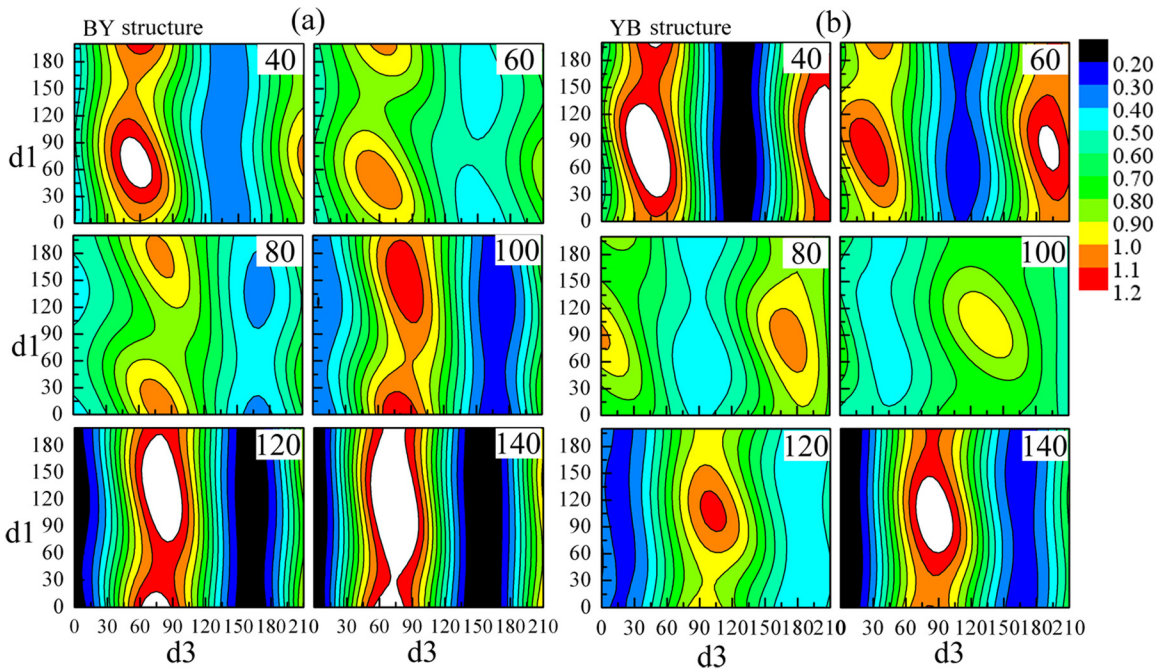

FIG. 5. Calculated emission intensities of BY devices (a) and YB devices (b). d2 was varied from 40 nm to 140 nm.

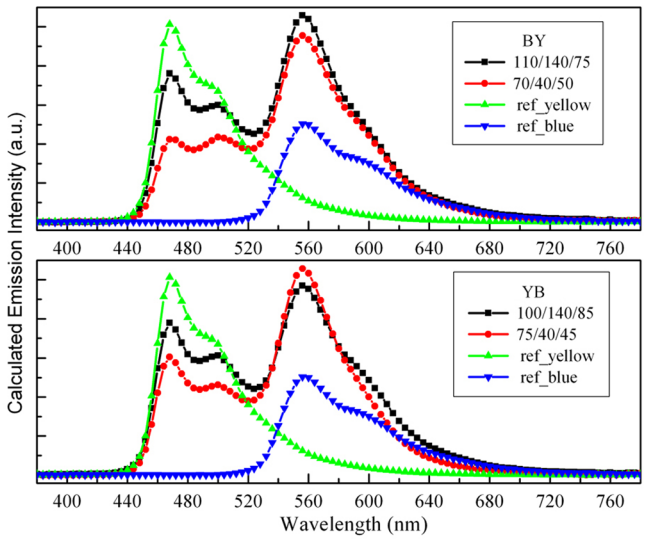

FIG. 6. Simulated spectra of devices in high intensity output positions.

45) and (100, 140, 85). We realized that in both devices, maximum I_{out}^{white} can be achieved when the total thickness of the organic layers (d1 + d2 + d3) is 160 and 325 nm. Including the thickness of the ITO anode (100 nm), the total thickness of the microcavities will be 260 and 425 nm. The corresponding resonant wavelengths at microcavity lengths of 260 and 425 nm are then calculated to be around 515 and 528 nm, respectively. These resonant wavelengths simulated from our tandem WOLED match emission from neither FIrpic (468 nm) nor PO-01 (560 nm) but are located between them. We then simulated the emission spectra of the BY and YB devices using Eq. (2) and observed that, for all of the high-intensity output positions (white parts in Fig. 5), the microcavity effect weakens the emission from the blue unit but strengthens that from the orange, as shown in Fig. 6. This is reasonable because the luminosity function of PO-01 (yellow) is higher than that of FIrpic (blue), so higher emission intensity can be obtained by enhancing the emission of PO-01.

2. Color rendering index

CRI is another important factor of high-performance tandem WOLEDs that needs to be considered. In this section, we calculated the CRI of the devices using the simulated spectra obtained from Eq. (2) by following traditional calculation steps.[23]

As shown in Fig. 7, in the BY devices, the regions with CRI > 60 (red or white parts) are confined in a small area when d2 is 40 nm. The high-CRI area expands gradually as d2 increases. When d2 is around 140 nm, the high-CRI area is mainly located at d3 < 80 nm and covers over 30% of the total area, which indicates that the CRI is insensitive to the thickness of both d1 and d3. In contrast, in the YB devices, the area with high CRI decreases as d2 increases and it is rather difficult to obtain a high-CRI area when d2 is 140 nm. To verify the accuracy of the CRI values, we compared our data with that calculated using SpectraWin® software, which is widely used to obtain the CRI of OLEDs. As can be seen in Table II, the CRI calculated with SpectraWin® software are consistent with our results, which demonstrates the validity of the simulation.

3. Angular emission properties

Typical microcavity structures will result in an angular dependence on the emitting color, which causes problems for display applications.[24] Spectra at different viewing angles can be calculated using Eq. (2) by changing θ so that the Commission Internationale de L'Eclairage (CIE)

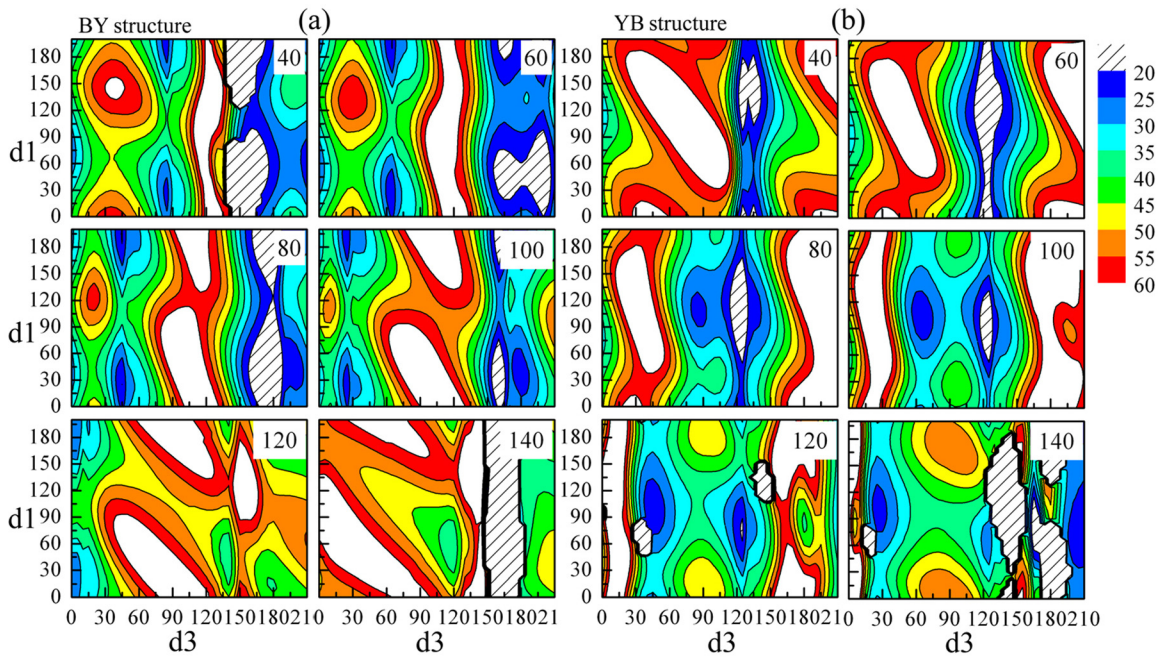

FIG. 7. The calculated CRI of BY devices (a) and YB devices (b). Regions filled with twills represent for devices whose CRI are failed to be calculated due to the relative CCT are out of calculated range.

TABLE II. Comparison of simulated CRI with that calculated using SpectraWin® software.

d1/d2/d3	40/60/40	40/60/60	40/60/80	60/60/40	60/60/60
Simulated results	55.06	57.20	56.43	56.84	64.41
SpectraWin® results	55	57	56	56	64

coordinates can be extracted. Thus, the change in color with viewing angle can be calculated using the following CIE color-difference equation:

$$\Delta E^*_{ab} = \sqrt{(L_1{}^* - L_2{}^*)^2 + (a_1{}^* - a_2{}^*)^2 + (b_1{}^* - b_2{}^*)^2}. \quad (4)$$

For each value of (d1, d2, d3), we can calculate the CIE color coordinates; namely, $(L_1{}^*, a_1{}^*, b_1{}^*)$ and $(L_2{}^*, a_2{}^*, b_2{}^*)$. Then, the total color differences can be obtained using Eq. (4). Fig. 8 depicts the color differences between viewing angles of 0° and 45°. The black regions represent the devices with smaller color difference, i.e., <12 NBS (National Bureau of Standards U.S.: averaged maximum acceptable difference in a series of measurements of a dye) at viewing angles of 0° and 45°. According to the perception degree between NBS unit and color difference,[25] when the color difference is larger than 12 NBS, the emission colors at viewing angles of 0° and 45° will be regarded as different colors. Thus, d1, d2, d3 should be confined to the black area to achieve good viewing characteristics.

In the BY devices, the black regions are mainly located at d1 > 120 nm and d3 < 150 nm for any value of d2. In the YB devices, the black area decreases in size as d2increases, which means the distance between different emission units (i.e., d2) should be smaller to achieve a wider viewing angle.

C. Design of high-performance tandem WOLEDs

In Sec. III B, we have separately studied the emission intensity, CRI and angular dependence performance of both BY and YB devices. To obtain a high-performance tandem WOLED, all of these factors need to be considered simultaneously. We then developed an image processing method to simultaneously consider emission intensity, CRI and angular dependence performance. Our target characteristics were: (i) device emission intensity of 1 or greater (see Sec. III B 1); (ii) CRI of 55 or higher (see Sec. III B 2); and (iii) color difference < 12 NBS between viewing angles of 0° and 45° (see Sec. III B 3). The selection of d1, d2, and d3 to simultaneously meet the above requirements is performed in Fig. 9(a) by (i) highlighting the qualified area (black color) in Figs. 5, 7, and 8 (step 1) and (ii) integrating these three black areas to determine the intersection area (step 2). Using this method, the intersection areas for the devices can be calculated (Fig. 9(b)). Fig. 9(b) reveals that, for YB structure, an intersection area can be obtained at relatively small d1 and d3 when d2 is 40 or 60 nm. This means the device has a small total thickness, which should allow low power consumption and driving voltage.[26] Here, it should be noted that the areas with extremely small values of d1 (areas near x-axes) were omitted to avoid unexpected severe electrode quenching of the excitons. Thus, the optimal area in Fig. 9(b) is that highlighted by a dashed rectangle so that, in addition to high light intensity, good CRI and weak angular dependence, low power consumption can also be realized. The highlighted regions in Fig. 9(b) represent the main contribution of this work. These regions indicate the optimal d1-d2-d3 combinations for tandem WOLEDs that can simultaneously give high harvest efficiency, high CRI, low angular dependence, and low power consumption. These findings provide clear design guidelines to achieve high-performance tandem WOLEDs. To verify

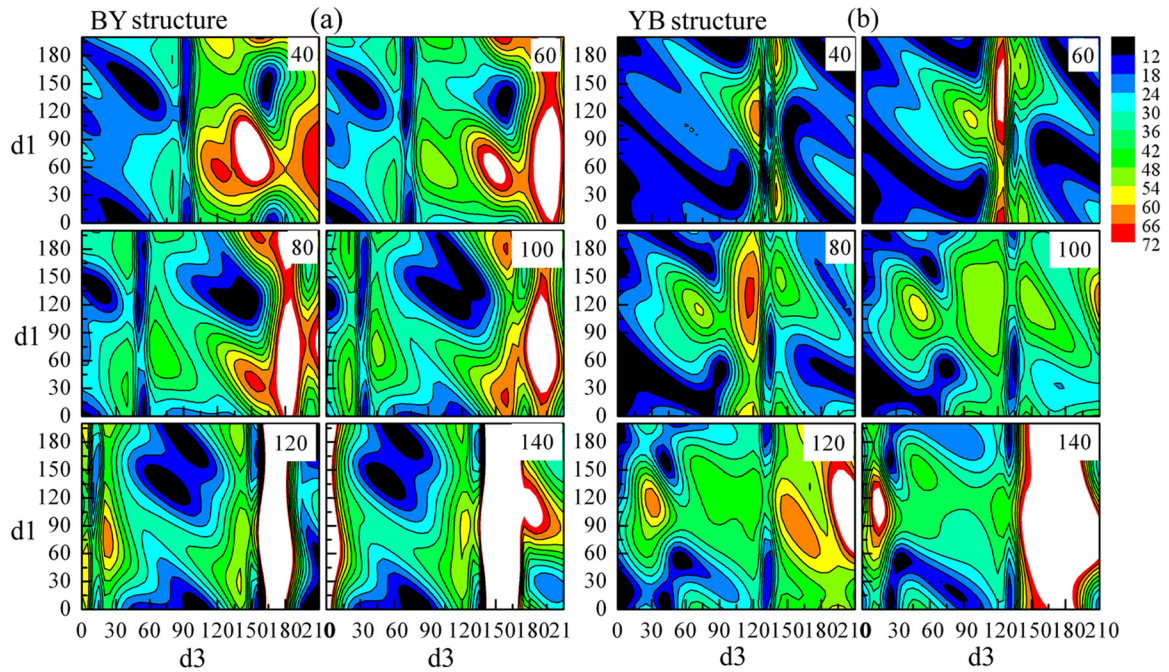

FIG. 8. The calculated color-differences between 0° and 45° viewing angle of BY devices (a) and YB devices (b).

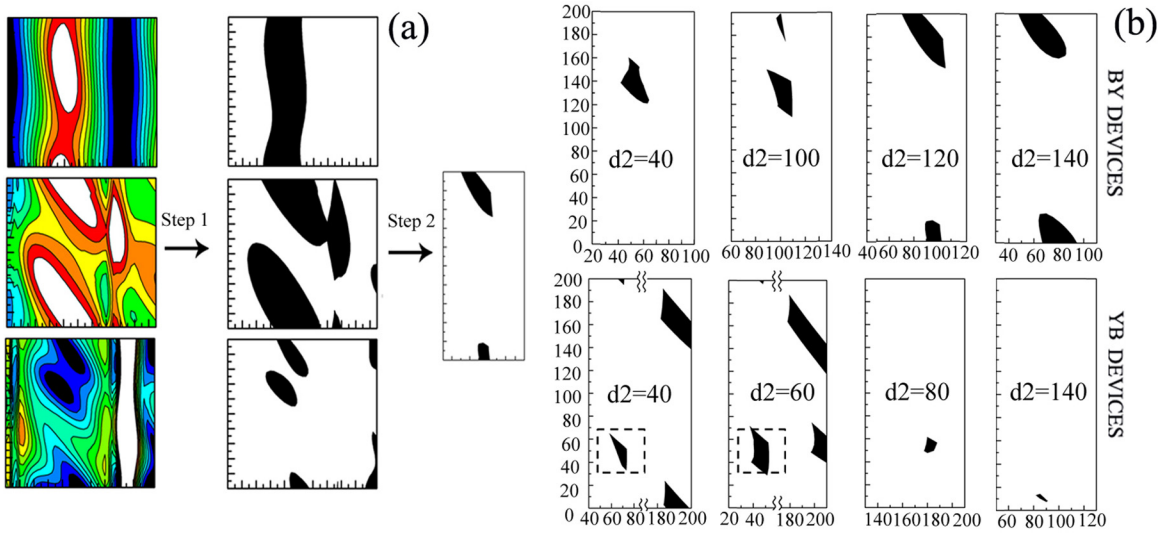

FIG. 9. (a) Demonstration of image processing steps. Here, BY devices with d2 = 120 nm are used as an example. (b) The intersection areas for BY and YB devices.

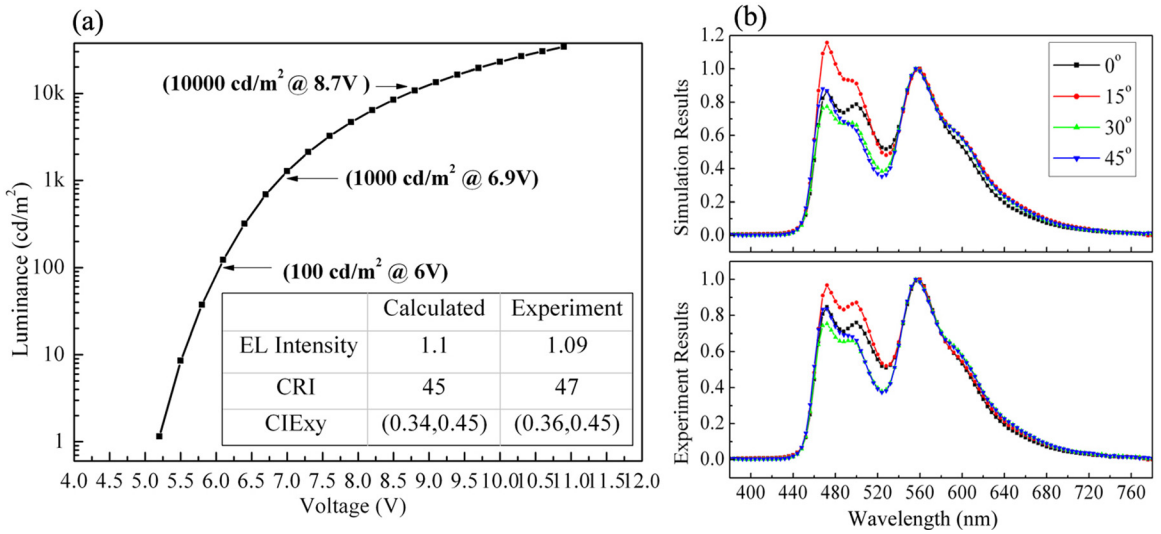

FIG. 10. (a) The voltage-luminance characteristics of fabricated tandem WOLED. The inset table shows the simulation and experiment results. (b) The angular emission properties of device B. The structure of device B is ITO/m-MTDATA(30)/Ir(ppz)$_3$(10)/CBP:PO-01(8 wt%,10)/Bphen(10)/Bphen:Cs_2CO_3(10)/TAPC:MoO_x(10)/TAPC(10)/mCP:Firpic(10 wt%,10)/Bphen(40)/LiF/Al.

our simulation results, a tandem WOLED (device B) was then fabricated using an optimal d1-d2-d3 combination. Fig. 10 compares the experimental data for this device with simulation results. The simulation results agree well with the experimental data for all of the calculated parameters (EL intensity, CRI, CIE, and power consumption), which further proves the reliability of our design method. The performance of device B is superior to that of most well-known organic heterojunction CGL-based WOLEDs.[10,27,28]

IV. CONCLUSIONS

In summary, we developed a strategy to realize tandem WOLEDs that simultaneously achieve high efficiency, high CRI, low angular dependence, and low power consumption by combining optical theory analysis with software simulation. The optimal location of the emission zones in tandem WOLEDs can be easily determined using an image processing method. Our findings reveal the utility of optical simulation of organic optoelectronic devices and pave the way for development of high-performance tandem WOLEDs.

ACKNOWLEDGMENTS

S.Y. programmed the codes and performed the software simulation. All authors are incorporated into the results discussion and manuscript preparation. We acknowledge all the researchers who participated in this work and whose names appear in references. We acknowledge funding for this research from the National Key Basic Research and Development Program of China (Grant No. 2010CB327701), and the National Natural Science Foundation of China (Grant No. 61275033).

[1]J. Kido, M. Kimura, and K. Nagai, Science **267**, 1332 (1995).
[2]H. Sasabe, K. Minamoto, Y.-J. Pu, and M. Hirasawa, Org. Electron. **13**, 2615 (2012).
[3]C.-C. Chang, J.-F. Chen, S.-W. Hwang, and C. H. Chen, Appl. Phys. Lett. **87**, 253501 (2005).
[4]T.-W. Lee, T. Noh, B.-K. Choi, M.-S. Kim, D. W. Shin, and J. Kido, Appl. Phys. Lett. **92**, 043301 (2008).
[5]L. S. Liao and K. P. Klubek, Appl. Phys. Lett. **92**, 223311 (2008).
[6]C.-W. Han, K.-M. Kim, S.-J. Bae, H.-S. Choi, J.-M. Lee, T.-S. Kim, Y.-H. Tak, S.-Y. Cha, and B.-C. Ahn, SID Symp. Dig. Tech. Pap. **43**, 279 (2012).
[7]S. Kawashima, K. Toyotaka, H. Shishido, H. Miyake, H. Kimura, S. Sanefuji, J. Koyama, S. Yamazaki, Y. Shima, and M. Katayama, in *13.5-Inch Quarter High Definition White Tandem OLED Display Using Crystalline In-Ga-Zn-Oxide Technology* (IEEE, 2012), p. 79.
[8]H. Miyake, H. Shishido, M. Sasaki, H. Ohara, H. Nowatari, T. Ushikubo, S. Seo, J. Koyama, S. Yamazaki, Y. Oikawa, H. Maruyama, and M. Sakakura, SID Symp. Dig. Tech. Pap. **41**, 253 (2010).
[9]J. P. Spindler and T. K. Hatwar, SID Symp. Dig. Tech. Pap. **38**, 89 (2007).
[10]Y. Chen and D. Ma, J. Mater. Chem. **22**, 18718 (2012).
[11]P. Chen, Q. Xue, W. Xie, Y. Duan, G. Xie, Y. Zhao, J. Hou, S. Liu, L. Zhang, and B. Li, Appl. Phys. Lett. **93**, 153508 (2008).
[12]L. Duan, T. Tsuboi, Y. Qiu, Y. Li, and G. Zhang, Optics Express **20**, 14564 (2012).
[13]F. Guo and D. Ma, Appl. Phys. Lett. **87**, 173510 (2005).
[14]X. Qi, M. Slootsky, and S. Forrest, Appl. Phys. Lett. **93**, 193306 (2008).
[15]S. Yue, S. Zhang, Z. Zhang, Y. Wu, P. Wang, R. Guo, Y. Chen, D. Qu, Q. Wu, Y. Zhao, and S. Liu, J. Lumin. **143**, 619 (2013).
[16]M. Cai, Z. Ye, T. Xiao, R. Liu, Y. Chen, R. W. Mayer, R. Biswas, K-M. Ho, S. Ruth, and J. Shinar, Adv. Mater. **24**, 4337 (2012).
[17]S. Gregor, R. Sebastian, C. R. Thomas, W. Karsten, and L. Karl, Adv. Funct. Mater. **19**, 1319 (2009).
[18]See supplementary material at http://dx.doi.org/10.1063/1.4897365 for brief investigation of down-conversion phenomenon.
[19]Z. B. Wang, M. G. Helander, X. F. Xu, D. P. Puzzo, J. Qiu, M. T. Greiner, and Z. H. Lu, J. Appl. Phys. **109**, 053107 (2011).
[20]H. Benisty, H. De Neve, and C. Weisbuch, IEEE J. Quantum Electron. **34**, 1612 (1998).
[21]X. Qi, N. Li, and S. R. Forrest, J. Appl. Phys. **107**, 014514 (2010).
[22]T.-Y. Cho, C.-L. Lin, and C.-C. Wu, Appl. Phys. Lett. **88**, 111106 (2006).
[23]W. Chen and L. Lu, Proc. SPIE **6782**, 678225 (2007).
[24]F.-S. Juang, L.-H. Laih, C.-J. Lin, and Y.-J. Hsu, Jpn. J. Appl. Phys., Part 1 **41**, 2787 (2002).
[25]A. C. Pero, J. Ignárcio, G. Giro, D. O. Mendoza-Marin, A. G. Paleari, and M. A. Compagnoni, Revista de Odontologia da UNESP **42**, 237 (2013).
[26]J. P. Dakin and R. G. Brown, *Handbook of Optoelectronics (two-volume set)* (CRC Press, 2006).
[27]Y. Chen, J. Chen, D. Ma, D. Yan, and L. Wang, Appl. Phys. Lett. **99**, 103304 (2011).
[28]Y. Chen, J. Chen, D. Ma, D. Yan, L. Wang, and F. Zhu, Appl. Phys. Lett. **98**, 243309 (2011).